inorganics

MDPI

Article

Alkali-Activated Metakaolin as a Zeolite-Like Binder for the Production of Adsorbents

Kristine Vegere [1,2], Laura Vitola [3,*], Pauls P. Argalis [1], Diana Bajare [3] and Andrey E. Krauklis [4]

1 Institute of General Chemical Engineering, Faculty of Materials Science and Applied Chemistry, Riga Technical University, P. Valdena street 3/7, LV-1048 Riga, Latvia; kristine.vegere@rtu.lv (K.V.); pargalis123@gmail.com (P.P.A.)
2 Water Research Laboratory, Faculty of Civil Engineering, Riga Technical University, P. Valdena street 1, LV-1048 Riga, Latvia
3 Department of Building Materials and Products, Riga Technical University, Kalku street 1, LV-1658 Riga, Latvia; diana.bajare@rtu.lv
4 Department of Materials and Nanotechnology, SINTEF Industry, 0314 Oslo, Norway; andykrauklis@gmail.com
* Correspondence: laura.vitola_1@rtu.lv; Tel.: +371-252-53294

Received: 11 September 2019; Accepted: 3 December 2019; Published: 6 December 2019

Abstract: This work reports and describes a novel alkali-activated metakaolin as a potential binder material for the granulation of zeolites, which are widely used as CO_2 adsorbents. The alkali-activated binders are zeolite-like materials, resulting in good material compatibility with zeolite-based adsorbents. A major problem during the granulation of zeolites is that their adsorption capacities decrease by about 15–20%, because typical binder materials (for example bentonite or kaolin clay) are inactive towards CO_2 adsorption. A possible pathway to solve this problem is to introduce a novel binder that is also able to sorb CO_2. In such a case, a binder plays a dual role, acting both as a binding material and as a sorbent. However, it is important that, alongside the adsorptive properties, a novel binder material must fulfil mechanical and morphological requirements. Thus, in this work, physical and mechanical properties of this novel binder for zeolite granulation for CO_2 adsorption are studied. Alkali-activated metakaolin was found to be efficient and competitive as a binder material, when mechanical and physical properties were concerned. The compressive strengths of most of the obtained binders reported in this work are above the compressive strength threshold of 10 MPa. The future work on this novel binder will be conducted, which includes granulation-related details and the CO_2 adsorptive properties of the novel binder material. Metakaolin was used as a precursor for alkali-activated binders. Binders were synthesized using varying molarity of a NaOH solution and at varying curing conditions. The final products were characterized using density measurements, compressive strength tests, X-ray diffraction (XRD), Fourier-transform infrared spectroscopy (FTIR), Brunauer–Emmett–Teller (BET) analysis, and scanning electron microscopy (SEM).

Keywords: alkali-activated binder; metakaolin; zeolites; CO_2 adsorbents; carbon dioxide; material characterization

1. Introduction

Low-calcium alkali-activated binders (AABs) or geopolymers are well-known zeolite-like materials, which have been studied as pH buffers and adsorbents for heavy metals [1–4]. It is proven that different types of zeolites in certain amounts (such as zeolite Na-A, hydrosodalite, zeolite X, faujasite, and analcime) can be formed as secondary alkali-activation products in the structure of an AAB [5–8]. Zeolites in the structure of an AAB might improve contaminant sorption effectiveness, i.e., in removal of heavy metals from wastewater [9,10], as well as removal of NH_4^+ [11], Ca^{2+} [10], and F^- [12]. Due to

relatively weakly bonded sodium and potassium ions in the N(K)–A–S–H gel structure (similar to zeolites), it is possible to provide alkali and H^+ ions exchange in water media [13].

Zeolites are also suitable for CO_2 adsorption, so they have been widely studied for biogas upgrading. During the biogas upgrading process, the main gases CO_2 and CH_4 are separated. Zeolites act as a CO_2-selective adsorbent in such applications. Therefore, improving CO_2 sorption efficiency is a crucial aspect of biogas upgrading. Zeolite-like binders, therefore, can provide such means by improving the CO_2 removal efficiency of an adsorbent. Biogas production occurs during the anaerobic digestion (AD) process. During the AD, waste is turned into a versatile source of energy and biofuel, reducing global dependence on fossil fuels [14–17]. The final product of a biogas upgrading process, termed biomethane, which contains more than 90% methane and is available as a vehicle fuel, can be fed into a natural gas grid or used for power generation. Production of biomethane from biogas is an eco-friendly and cost-effective process that offers positive environmental uneconomic impact in the case of fuel independence [18–21]. The efficiency of biogas upgrading, in which carbon dioxide should be separated from methane, depends on granulated adsorbent structures, material types, structuring methods, and binders. The structuring or granulation with binder agents is performed before the use of zeolite in gas adsorption columns. This results in reduced CO_2 adsorption capacity and may also result in insufficient mechanical properties. Usually, binders do not possess an ability to sorb gas, and therefore, they may reduce an adsorption capacity even up to 20% after structuring [22] and/or clogging pores [23]. Beside adsorption properties, structuring processes also affect the mechanical strength of granules [24,25]. The binder type and the method of a structuring or granulation process dramatically influence physical and chemical properties of the resulting granules [26].

Routes to combine zeolites with AABs have recently attracted increasing research interest from various groups [5,27–29]. Low-calcium AABs mainly consist of cross-linked zeolite-like aluminosilicate gel (N–A–S–H gel) [30] and have been used for various applications, including membranes and catalysts [31–33]. In various publications, transformations of AABs into zeolites have been investigated [34–36]. For example, adsorption properties of CO_2 on AAB materials were studied by Minelli et al. [36]. Additionally, geopolymer-based composite materials as CO_2 adsorbents were studied by Papa et al. and Minelli et al. [37–39]. There is also a very recent work by Medri et al. on the production methods of metakaolin (MK)-based geopolymer beads [40]. These recent studies suggest that zeolite-like binders are a potential route of improving the CO_2 sorption capacity of zeolitic granules. However, understanding the effect of curing conditions on microstructures, physical properties, and especially mechanical properties of the obtained final products is still lacking. Compressive properties are of high importance for sorbent granules due to mechanical loading in the adsorption column for a long operational period of at least 1–3 years. In this paper, novel alkali-activated MK binders obtained at various curing conditions were reported and described. Various curing conditions affected the final product and therefore were investigated, and final products obtained under different curing conditions were compared in terms of microstructure and mechanical performance. Typical zeolite granules should have a compressive strength of at least 10 MPa for biogas upgrading columns. The compressive strengths of most of the obtained binders reported in this work were above this compressive strength threshold.

2. Results and Discussion

2.1. Density and Compressive Strength

The material densities, the total porosities, and the compressive strengths of the monolithic AABs are shown in Table 1. According to the obtained results, the material densities of the AABs ranged from 1230 up to 1535 kg/m^3, depending on binder composition and curing conditions, which were higher than those of zeolite 4A granules with an average density of 950–1150 kg/m^3 [26]. As seen in Table 1, the samples of series M8 exhibited lower material densities (1230–1255 kg/m^3) compared to

the samples of series M10 (material density: 1530–1535 kg/m^3), while the samples of series M6 had material densities in a range of 1285–1315 kg/m^3.

Table 1. Material densities, total porosities, and compressive strengths of the studied alkali-activated binders (AABs).

Composition		Material Density, kg/m^3	Total Porosity, %	Compressive Strength, MPa
M6	**CC**	1315 ± 22	37.9 ± 1.1	10.8 ± 1.3
	RC	1285 ± 29	36.4 ± 1.4	15.1 ± 1.3
	CO_2	1285 ± 16	37.9 ± 0.8	18.9 ± 2.4
M8	**CC**	1255 ± 47	40.9 ± 2.2	17.3 ± 0.7
	RC	1245 ± 16	40.6 ± 0.8	19.1 ± 1.5
	CO_2	1230 ± 34	41.7 ± 1.6	20.8 ± 1.7
M10	**CC**	1535 ± 11	28.9 ± 0.5	9.4 ± 0.7
	RC	1530 ± 9	28.7 ± 0.4	20.3 ± 1.7
	CO_2	1535 ± 7	28.7 ± 0.3	14.9 ± 0.9

The highest total porosity from 40.6% to 41.7% was found for series M8, while the lowest total porosity (28.7–28.9%) was observed for series M10, but series M6 presented the total porosity depending on the curing type in a range from 36.4% to 37.9%. It is clearly visible that the total porosity was not strongly affected by the type of curing, but it strongly depended on the molarity of the used alkali-activation solution. The reason for this is not obvious, but the authors think that this may be linked to a few differences in the mineralogical microstructure of the final products obtained. For instance, as will be explained later in more detail, different types of zeolites were formed at various conditions, which had different crystal sizes and different packing. The correlation is not clear, but it can be speculated that some amount of relatively small zeolite crystals (like zeolite 4A) might provide a denser AAB structure, also affecting the porosity and the compressive strength of the final product.

As seen in Table 1 and Figure 1, the studied AABs had compressive strengths ranging from 9.4 to 20.8 MPa, depending on binder composition and curing conditions. Özen et al. reported that the compressive strengths of natural zeolite-based geopolymers were in a range between 6.7 and 42.0 MPa [41,42], which agrees with the experimental results presented here. Mechanical properties are very important for zeolite granules due to abrupt gas and packing movements and other mechanical influences in the adsorption column during the long-time operational period (at least 1–3 years). Typical zeolite granules should have compressive strengths of at least 10 MPa for biogas upgrading columns. The compressive strengths of most of the obtained binders reported in this work were above this compressive strength threshold.

The samples (M6-CC, M8-CC, and M10-CC) that were kept in the CC (at 85 °C with a humidity of >95%) presented the lowest compressive strength. On the contrary, the samples that were kept in a CO_2-rich environment (CO_2-type, at 22 ± 2 °C with a humidity of 5%), in the case of series M8, presented the highest compressive strength. After curing at RCs, series M10 showed the highest compressive strength.

Among the three obtained series, the compressive strengths of series M8 for all the three types i.e., CC-, RC-, or CO_2-type samples, were the most stable (least affected), when the environmental conditions (temperature, moisture, and CO_2 content) were changed.

For the room-curing conditions (RC-type), the compressive strength of the final product increased with the molarity of the activation solution, which were 15.1 ± 1.3, 19.1 ± 1.5, and 20.3 ± 1.7 MPa for M6-RC, M8-RC, and M10-RC, respectively.

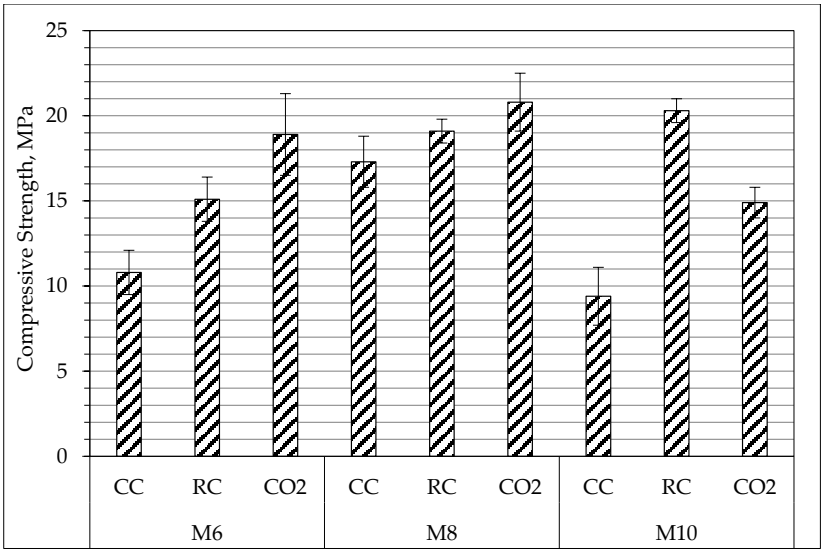

Figure 1. Compressive strength results of the studied AABs.

2.2. X-Ray Diffraction

The AABs made of MK had a crystalline phase from the raw MK (quartz). The new crystalline phase after alkali activation strongly depended on the molarity of the used NaOH solution (alkali-activation solution).

In accordance with the XRD results (Figure 2), apart from the amorphous phase, the raw MK had some crystalline phases of quartz (SiO_2) and mica ($KAl(Mg_{0.2}Al_{0.8})(Al_{0.21}Si_{1.83})_2O_{10}(OH)_2$). The halo from 15° to 25° found in the raw MK corresponded to the amorphous aluminium silicates (Figure 2). In all the cases, this halo moved towards the region of a higher degree (20–30°) after the alkali activation, which corresponded to the N–A–S–H gel (main alkali-activation reaction product) formation [42].

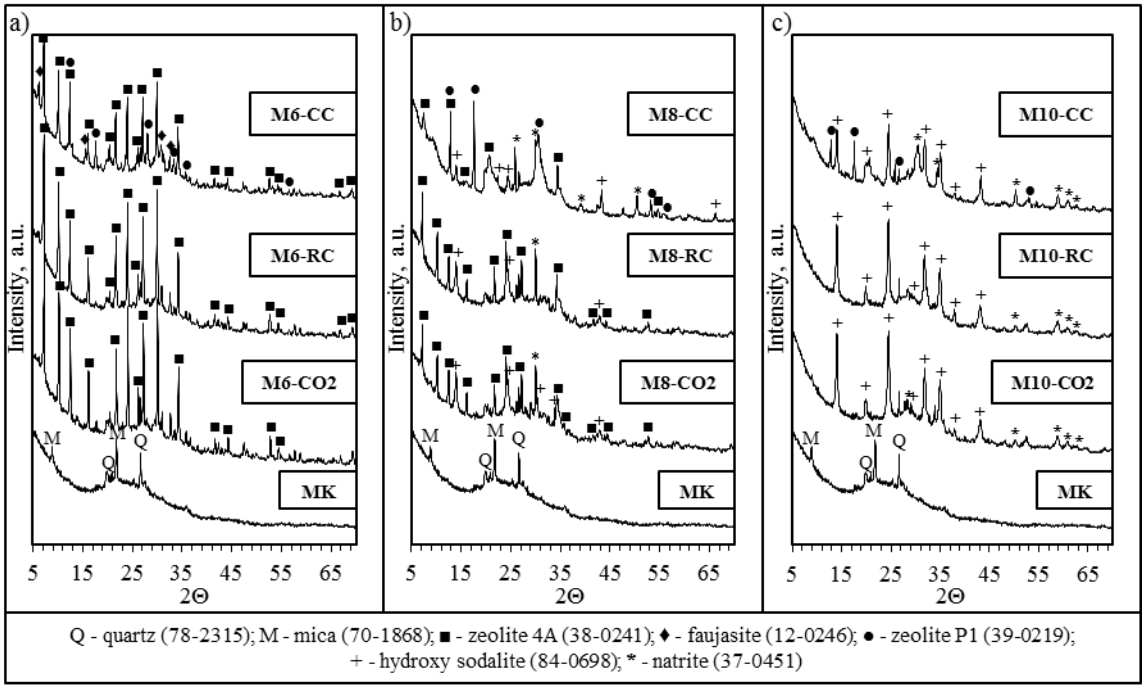

Figure 2. X-ray diffraction (XRD) of the studied alkali-activated binders (AABs). (**a**) M6 samples; (**b**) M8 samples; (**c**) M10 samples.

As observed in Figure 2a, the AABs of series M6 indicated a crystalline phase of zeolite 4A ($Na_2Al_2Si_{1.85}O_{7.7}{\cdot}5.1H_2O$; Si/Al = 0.9, Si/Na = 0.9, and Al/Na = 1) and zeolite P1 ($Na_6Al_6Si_{10}O_{32}{\cdot}12H_2O$; Si/Al = 0.6, Si/Na = 0.6, and Al/Na = 1). Additionally, M6-CC contained a small amount of faujasite ($Na_2Al_2Si_{2.4}O_{8.8}{\cdot}6.7H_2O$; Si/Al = 1.2, Si/Na = 1.2, and Al/Na = 1).

Moreover, the AABs of series M8 (Figure 2b) had less of the crystalline phase of zeolite 4A ($Na_2Al_2Si_{1.85}O_{7.7}{\cdot}5.1H_2O$; Si/Al = 0.9, Si/Na = 0.9, and Al/Na = 1) compared to the AAB series M6, but due to a higher amount of sodium in the composition, this series indicated the presence of natrite (Na_2CO_3). In addition, a crystalline phase of sodium aluminum silicate hydrate or hydroxy sodalite ($Na_{3.68}Al_{3.6}Si_{8.4}O_{24}{\cdot}H_2O$; Si/Al = 2.3, Si/Na = 2.3, and Al/Na = 1) was detected.

In the case of series M10, the studied AABs presented the presence of hydroxy sodalite ($Na_{3.68}Al_{3.6}Si_{8.4}O_{24}{\cdot}H_2O$; Si/Al = 2.3, Si/Na = 2.3, and Al/Na = 1), and M10-CC also showed some crystalline phase of zeolite P1 ($Na_6Al_6Si_{10}O_{32}{\cdot}12H_2O$; Si/Al = 0.6, Si/Na = 0.6, and Al/Na = 1) and natrite (Na_2CO_3) (Figure 2c).

The curing conditions of AABs after alkali activation also impacted the formation of zeolites in the structures of AABs. In Figure 2, it can be seen that the curing samples (M6-CC, M8-CC, and M10-CC) after alkali activation six days before testing in the CC (at 85 °C with a humidity of >95%) provided the formation of zeolite P1 in all the cases. In the case of M6-CC compared with M6-RC and M6-CO_2 along with the formation of zeolite P1, some new crystalline phases of faujasite were formed. The high CO_2 curing environment (at 22 ± 2 °C with a humidity of 5%) had no noteworthy impact on the mineralogical composition of the AABs in the curing samples (M6-CO_2, M8-CO_2, and M10-CO_2).

The decrease of the compressive strengths of the CC-type samples comparing to those of the RC-type samples can be explained by structural changes caused by the formation of zeolite P1. The formation of zeolite P1 resulted in a higher decrease of compressive strength than the decrease in the formation of zeolite 4A because of the difference in volumes of zeolite crystals. The sizes of zeolite P1 crystals in the alkali-activated MK were about 4–8 μm, while those of the crystals of zeolite 4A were up to 2 μm.

2.3. FTIR

The FTIR spectra of the MK are presented in Figure 3, and wavenumbers are shown in Table 2. These spectra consisted of two main intense bands at 1039 cm^{-1}, which corresponded to the asymmetric stretching vibrations of T–O (where T was Si or Al), and at 478 cm^{-1}, which was assigned to the internal T–O bending vibrations [43].

Table 2. Assignments of FTIR analysis for the studied AABs.

Wavenumbers, cm^{-1}										Assignments	Ref.
MK	MK6			MK8			MK10				
	CC	RC	CO_2	CC	RC	CO_2	CC	RC	CO_2		
1638	1648	1654	1648	1655	1638	1638	1654	1638	1650	O–H bending vibrations	[5,43]
-	1466	1459	1449	1440	1458	1458	1458	1458	1458	ν_3 C–O (CO_3^{2-})	[41]
1039	1010	1007	1007	1019	1001	1002	1011	997	997	ν_3 T–O (T = Al, Si)	[20,42]
-	-	-	836	-	-	836	-	-	836	ν_2 C–O (CO_3^{2-})	[41]
777	-	-	-	-	-	-	-	-	-	ν_1 Si–O	[42]
-	669	670	702	704	669	704	669	663	622	ν_4 Si–O–Si	[41,42]
622	558	558	558	517	558	615	-	-	-	ν_4 Al–O–Al	[5,20,44]
478	464	466	466	459	460	462	459	459	459	ν_4 Si–O	[41,42]

After the alkali activation, in all the cases, the band at 1039 cm^{-1} moved to a lower wavenumber due to the N–A–S–H gel formation [20,43]. A band at 558–615 cm^{-1} appeared intense after the alkali activation and corresponded to vibrations of a double four-membered ring in the zeolite 4A framework [5].

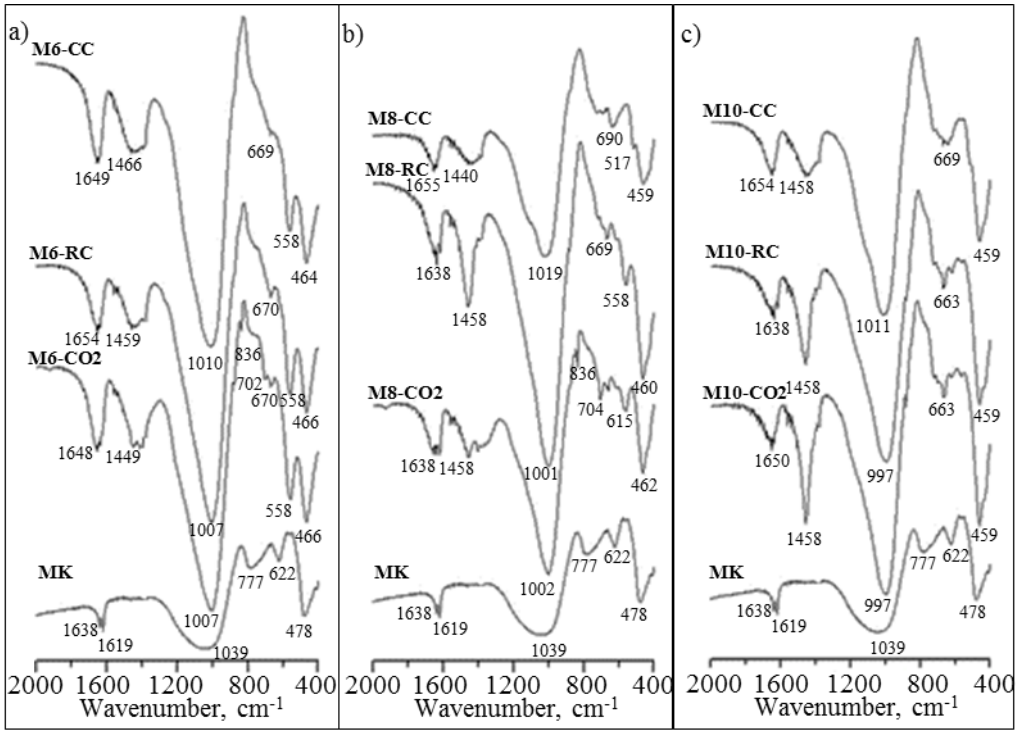

Figure 3. FTIR transmittance spectra of the studied AABs.

Bands appearing at 1619–1655 cm^{-1} were attributed to the O–H bending vibrations in water molecules [5,44,45].

As presented in Figure 3, a higher-molarity NaOH solution (10 M) caused a more intense formation of carbonates, and series M10 presented a more intense peak at 1458 cm^{-1} (indicating the C–O asymmetric stretching) compared to series M6 and M8. At the same time, a lower-molarity NaOH solution (6 and 8 M) caused an intense formation of a zeolite 4A phase, which corresponded to a ν_4 Al–O–Al peak at 517–615 cm^{-1}. These results are consistent with the XRD results described above.

No significant difference in the presence of carbonates was observed between the CO_2-type, RC-type, and CC-type specimens, considering they were prepared at the same NaOH molarities. In other words, using an activation solution of the same molarity, i.e., 8 M NaOH, but varying the environment (after demoulding and until testing the specimens), did not seem to affect the presence of carbonates, as indicated by the XRD and FTIR spectra (Figures 2 and 3). The reason for the absence of higher carbonate content is not completely clear, but perhaps at this stage and at the studied conditions, further carbonization does not occur in the studied AABs.

2.4. BET Analysis

The specific surface area was determined only for the room-cured specimens due to technical limitations. However, since curing at RCs (RC-type) is the cheapest route and, therefore, is likely to be more beneficial in an industrial setting, the RC-type specimens were chosen for BET testing. Additionally, the total porosity (Table 1) was not strongly affected by the type of curing method but was strongly dependent on the molarity of the used alkali-activation solution. Therefore, it seems that comparing influence of alkali-activation molarity is more relevant. The specific surface areas of M6-RC, M8-RC, and M10-RC were 8.98, 2.36, and 2.98 m^2/g, respectively. The specific surface area of M6-RC was the highest and was approximately three times higher than the rest of the obtained AABs. The higher surface area may be explained by a higher zeolite content. The surface area of the material is important in adsorption applications. Thus, the molarity of an activation solution plays a crucial role in the design of binders, when adsorption characteristics of binders are important. The AABs obtained

via the activation with a 6 M hydroxide solution is a promising material among the studied AABs, exhibiting the highest specific surface area, which is an important parameter for sorption. The increase in the binder content causes a decrease in the surface area of granules [46], and thus, it is important to choose a binder with a high specific surface area. The pore size distributions of the AABs were compared in detail, as shown in Figure 4. All the samples developed micropores and mesopores within a range of 1–36 nm.

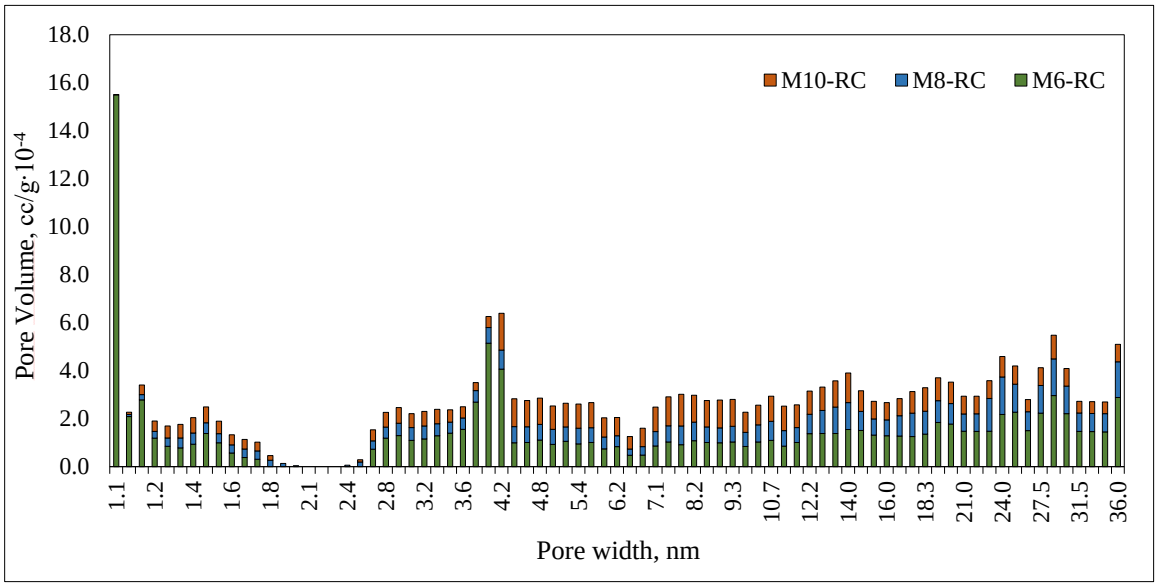

Figure 4. Pore volume and pore width determined for the room-cured specimens of M6-RC, M8-RC, and M10-RC.

2.5. SEM Analysis

SEM was performed only for the specimens of series M8 due to technical limitations. SEM was performed at the last stage of the investigation, and thus series M8 was selected. The reason for choosing series M8 was that this series showed advantages over the other types due to its excellent compressive strength being least affected if the environmental conditions (RC-type, CC-type, and CO_2-type) were changed. The microstructures of the studied AABs are shown in Figure 5 for M8-CC, M8-RC, and M8-CO_2. It was determined that the type of curing (CC, RC, and CO_2) had no impact on the density of the AAB microstructure.

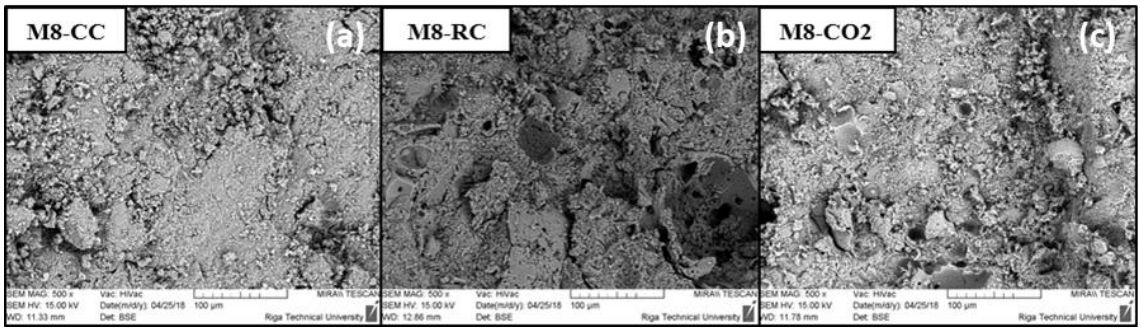

Figure 5. SEM micrographs presenting the microstructures of the studied AABs (series M8) depending on curing conditions (curing chamber, room conditions, and high CO_2 environment): (**a**) M8-CC; (**b**) M8-RC; (**c**) M8-CO_2.

Meanwhile, it can be argued that the curing type (CC, RC, and CO_2) impacted the formation of crystalline compounds (zeolites) in the microstructures of the studied AABs (Figure 6). According to

the SEM micrographs, all the studied AABs (M8-CC, M8-RC, and M8-CO_2) along with the main alkali activation reaction product (N–A–S–H gel) also presented some crystals (size: 1–2 μm), which were both spherical and cubic. This observation indicated that both hydroxy sodalite and zeolite 4A were present after the alkali activation of MK in series M8.

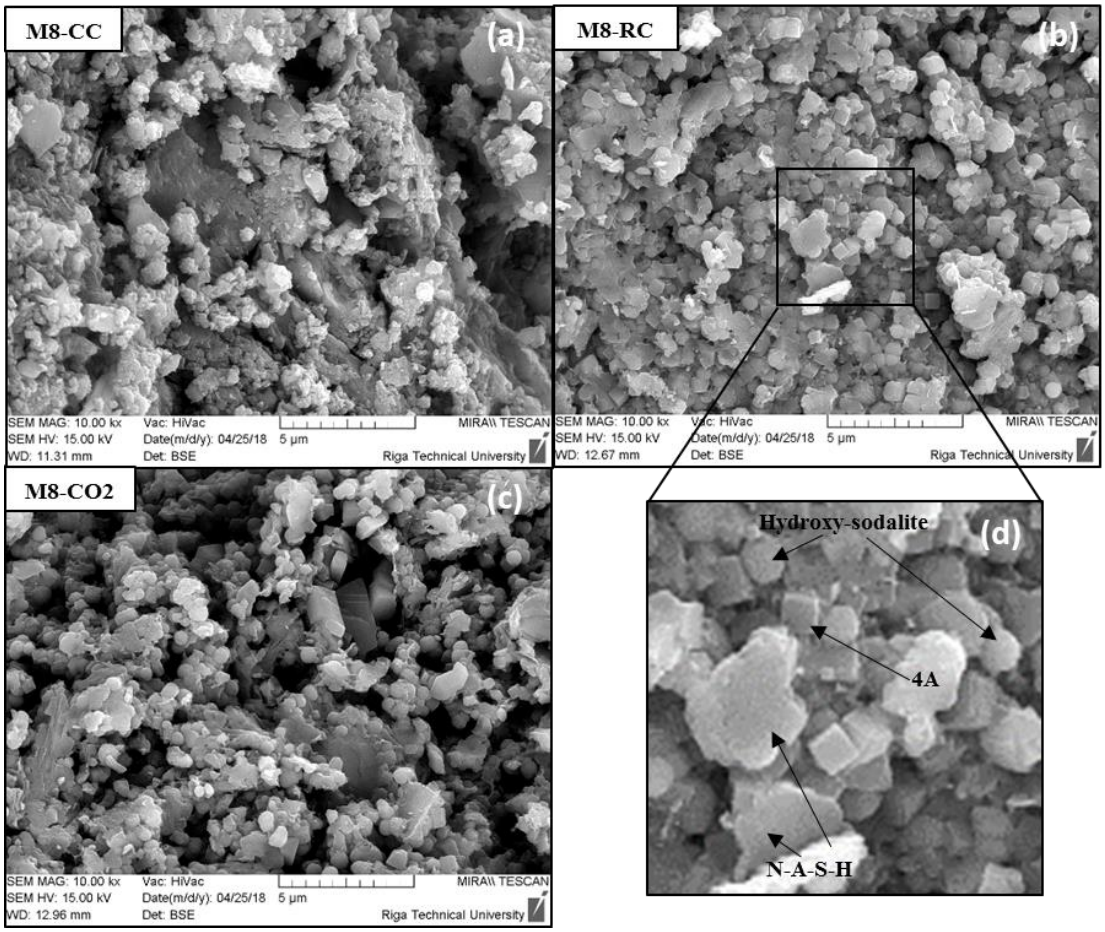

Figure 6. SEM micrographs of the studied AABs (series M8) indicating the presence of zeolites depending on curing conditions (curing chamber, room conditions, and high CO_2 environment): (**a**) M8-CC; (**b**) M8-RC; (**c**) M8-CO_2. (**d**) SEM micrograph of the area indicated by a rectangular in (**b**) enlarged by a factor of two.

2.6. Discussion on the Choice of Optimal Binder for Sorptive Applications

For granular sorbents, sufficient mechanical strength and good sorption characteristics are critically important. In this work, compressive strength and other parameters such as density, porosity, and specific surface area were studied. Sorption capacity was not covered herein and will be studied in future work. Microstructure, mineralogical composition, and their effects on final properties of the product were investigated and discussed.

Specific surface area was determined only for the RC-type series and was highest for M6-RC (8.98 m^2/g). However, it should be noted that the main parameter that was investigated in this work was mechanical performance. Nevertheless, in a future study on sorptive properties, M6-RC should also be addressed, since it also fulfilled the mechanical requirement of a compressive strength of 15.1 ± 1.3 MPa, which was above the threshold.

For good mechanical performance, typical zeolite granules should reach at least 10 MPa in compressive strength, if they are to be used in biogas upgrading applications. All the obtained AABs had a compressive strength within a range from 9.4 up to 20.8 MPa, depending on binder composition

and applied curing conditions. All of the obtained products, except for M6-CC (compressive strength: 10.8 ± 1.3 MPa) and M10-CC (compressive strength: 9.4 ± 0.7 MPa), confidently met the mechanical requirements of a sorbent granule. Based on these findings, the CC type of curing was not the most optimal for producing sorbent binders. However, both the RCs and carbon dioxide (CO_2) curing methods provided final binder products with a good mechanical strength. Low compressive strength in the case of the CC-type samples can be explained with the microstructure and the mineralogical composition of the final product. In the CC-type products, the formation of zeolite P1 caused a pronounced reduction in compressive strength due to the P1 crystals having a larger volume than 4A. For the CO_2-rich environment (CO_2-type), M6-CO_2 (compressive strength: 18.9 ± 2.4 MPa) and M8-CO_2 (compressive strength: 20.8 ± 1.7 MPa) presented good mechanical characteristics, whereas M10-CO_2 (compressive strength: 14.9 ± 0.9 MPa) had a significantly lower strength. The AABs cured in room curing conditions (RC) showed sufficient mechanical performance. Furthermore, the compressive strength of the final RC-type product increased with the molarity of the activation solution. The strengths of the final RC-type products were 15.1 ± 1.3, 19.1 ± 1.5, and 20.3 ± 1.7 MPa for M6-RC, M8-RC, and M10-RC, respectively.

In addition, the total porosity was not strongly affected by the type of curing method but was strongly dependent on the molarity of the used alkali-activation solution. The M8 samples showed the highest porosity, but the reason for this was not completely clear. The authors think that this is due to a few differences in the mineralogical microstructure of the final products obtained. Different types of zeolites were formed due to activation with NaOH solutions of different molarities, which likely influenced crystal size and packing in the final product. As the authors speculated earlier, it is likely that some amount of relatively small zeolite crystals might provide a denser AAB structure, also affecting the porosity of the final product.

According to the FTIR results, higher molarity (10 M) of a NaOH solution resulted in a product with a more intensive formation of carbonates (1458 cm^{-1}). The lower-molarity NaOH solutions (6 and 8 M) caused an intense formation of a zeolite 4A (517–615 cm^{-1}), which made these alkali activation conditions more favorable for the application. Based on both the zeolitic A microstructure (XRD, FTIR, and SEM results) and the mechanical performance (compressive strength), the most appropriate activation method of AABs was to use the 8 M alkali activation solution, followed by the RCs curing. Furthermore, curing at room conditions (RC-type) is the cheapest route and, therefore, is likely to be more beneficial in an industrial setting.

Optimal conditions were found for obtaining AABs for the studied application. However, for sorptive applications, future work on the novel binder is required and will be conducted. This will include granulation-related details and the CO_2 sorptive properties of novel binder materials.

3. Materials and Methods

3.1. Raw Materials

As an aluminium silicate source for AAB production, a commercially available MK produced by LTD Stikloporas (Druskininkai, Lithuania) was used. The used MK was a by-product from the final stage of the expanded glass granules' production, when kaolinite clay powder was used as a substance for antiagglomeration at a temperature of 850 °C for 40–50 min. The chemical composition of MK is given in Table 3. Sodium hydroxide solutions with molarities of 6, 8, and 10 M were used as an alkali-activation solution for binder production. Figure 7 shows the typical morphology of the studied MK consisting of thin flakes sized between 1 and 5 μm.

Table 3. Chemical composition of solid raw materials shown as weight percentage (unit: %).

Compound	Al_2O_3	SiO_2	CaO	TiO_2	MgO	Fe_2O_3	Na_2O	Others	LOI, 1000 °C
MK	34.2	51.8	0.1	0.6	0.1	0.5	0.6	12.1	11.9

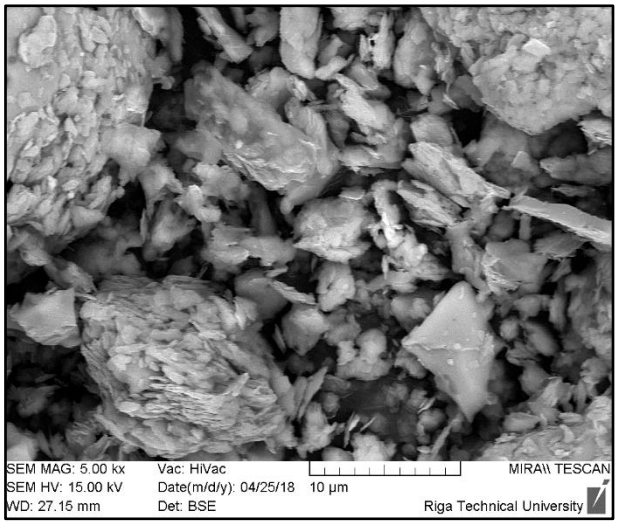

Figure 7. SEM micrograph showing the microstructure of the raw metakaolin. A magnification of 5000× was used.

3.2. Mixture Design and Sample Preparation

The mixture-design-related details of AABs are provided in Table 4; in all the cases, a Si/Al ratio was 1.3. An alkali-activation solution/metakaolin (AAS/MK) ratio of 0.6 was chosen to ensure the optimal workability. The blend of MK and the activation solution (NaOH solution) was mixed for 8 min using a mechanical mixer. After that, moulds (20 mm × 20 mm × 20 mm) were filled and kept at room temperature (20–23 °C) for 2 h. The specimens were then put in an oven and kept at 85 °C for 20 h with a humidity of >95%.

Table 4. Compositions of the studied alkali-activated metakaolin.

Composition		Raw Materials, Mass Parts				Curing Condition 2nd–7th Day After Making		
		MK	NaOH Solution			Climate Chamber	Room Conditions	High CO_2 Environment
Series	Type		6 M	8 M	10 M			
M6	CC	1	0.6			+		
	RC	1	0.6				+	
	CO_2	1	0.6					+
M8	CC	1		0.6		+		
	RC	1		0.6			+	
	CO_2	1		0.6				+
M10	CC	1			0.6	+		
	RC	1			0.6		+	
	CO_2	1			0.6			+

Three series of AAB samples were prepared:

- Curing chamber (CC)-type: M6-CC, M8-CC, and M10-CC. After demoulding, the specimens were kept in a CC (at 85 °C with a humidity of >95%) until testing;
- Room condition (RC)-type: M6-RC, M8-RC, and M10-RC. After demoulding the specimens were kept at RCs (at 22 ± 2 °C with a humidity of 20%) until testing;

- CO_2-type: M6-CO_2, M8-CO_2, and M10-CO_2. After demoulding, the specimens were kept in the high CO_2 environment (at 22 ± 2 °C with a humidity of 5%) until testing. A high CO_2 environment was chosen, because of the required knowledge about material characteristics within CO_2, to identify whether carbonization could occur. The high CO_2 environment and the carbonization aspect could potentially influence mechanical properties of the final binder product.

After mechanical tests (on day 7), the specimens were ground into powder for the next material characterization experiments: X-ray diffraction (XRD), Fourier-transform infrared spectroscopy (FTIR), and specific surface area analysis (based on the Brunauer–Emmett–Teller (BET) theory).

3.3. Characterization Techniques

The compressive strengths of six parallel samples (cubic AAB specimens) of each series with a dimension of 20 mm × 20 mm × 20 mm were tested using a universal testing system Zwick Z100 (ZwickRoell, Kennesaw, GA, USA) with a testing speed of 0.5 m/min. The cubic specimens were also tested to detect the material densities, which were calculated as the masses of the samples divided by their respective volume. The compressive strengths of six parallel samples of each series with a dimension of 20 mm × 20 mm × 20 mm were tested by using the universal testing system Zwick Z100 with a testing speed of 0.5 m/min. Total porosity was obtained from the specific gravity obtained by a Le Chatelier flask, in accordance with ASTM C188.

The XRD characterization of the AABs powders was performed with a BRUKER-AXS D8 ADVANCE X-ray diffractometer (Bruker, Billerica, MA, USA) and using CuKα1 and CuKα2 radiation at a 2θ range of 5–70°.

A Varian FTS 800 FT-IR Scimitar Series spectrometer (Varian, Palo Alto, CA, USA) was used to obtain FTIR spectra in a range from 2000 to 400 cm^{-1} with a resolution of 4 cm^{-1}. For the FTIR measurements, 1 mg of each sample was mixed with 300 mg of KBr separately.

The specific surface area and the porosity of the AABs was studied via N_2 sorption and desorption based on the BET theory [47]. The specific surface area was measured using the QUADRASORB SI (Quantachrome Instruments, Boynton Beach, FL, USA) equipment. Degassing was performed to free the surface of the specimens from moisture and other contaminants, according to the International Union of Pure and Applied Chemistry (IUPAC) guidelines. The degassing was performed for 24 h at 100 °C using Autosorb Degasser model AD-9.

The scanning electron microscopy (SEM) of the AABs microstructures was performed using Mira/LMU (Tescan, Brno, Czech Republic).

4. Conclusions

For granular sorbents, a sufficient mechanical performance is a critical parameter. In this work, physical and mechanical characteristics of MK-based AABs were studied and linked to the microstructure and the mineralogical composition of the final product. The molarity of the alkali activation solution (6, 8, and 10 M) and curing conditions (RC, CC, and CO_2) had crucial roles that resulted in the varying properties of the obtained AABs. For a good mechanical performance in biogas upgrading applications, typical zeolite granules should reach at least 10 MPa in compressive strength. All of the products, except for M6-CC (compressive strength: 10.8 ± 1.3 MPa) and M10-CC (compressive strength: 9.4 ± 0.7 MPa), confidently met the mechanical requirements of a typical sorbent material, and even M8-CO_2 had a compressive strength of 20.8 MPa. Low compressive strength for the CC-type samples was explained with the formation of zeolite P1, which had a larger crystal volume than 4A.

The molarity of an alkali activation solution and the curing method impacted the type of zeolite that was formed. Lower molarity of a NaOH solution (6 M) resulted in a zeolite 4A formation during alkali activation. Increasing the molarity (from 6 to 8 M and further increased to 10 M) of the solution caused the formation of hydroxy sodalite instead of zeolite 4A. Moreover, because of the high molarity of the NaOH solution (10 M), free alkalis may take part in the carbonation reaction; as a result, a crystalline phase of natrite was formed. In addition, the prolonged curing of the binders at 80 °C and

the high humidity caused the formation of zeolite P1. The total porosity was not strongly affected by the type of curing but was strongly dependent on the molarity of the used alkali-activation solution.

Based on both the zeolitic microstructure (XRD, FTIR, and SEM results) and the mechanical performance, the most appropriate conditions for the synthesis of AABs for the studied application were using an 8 M activation solution and room curing (RC-type). Series M8 showed advantages over the other series in terms of the mechanical properties and the amount of zeolite A in the final product. Furthermore, the room curing conditions are the cheapest and, therefore, are likely to be more beneficial in an industrial setting.

Author Contributions: Conceptualization, K.V. and L.V.; methodology, K.V. and L.V.; formal analysis, P.P.A. and L.V.; investigation, P.P.A., L.V., K.V., D.B., and A.E.K.; resources, K.V. and D.B.; data curation, L.V. and K.V.; writing of the original draft preparation, L.V., K.V., and A.E.K.; writing of review and editing, L.V., K.V., D.B., and A.E.K.; supervision, D.B. and A.E.K.; project administration, K.V.; funding acquisition, K.V.

Funding: This research was funded by the European Regional Development Fund within the Activity 1.1.1.2 "Post-doctoral Research Aid" of the Specific Aid Objective 1.1.1 of the Operational Programme "Growth and Employment" (No. 1.1.1.2/VIAA/1/16/116, "The development of biomethane production technologies").

Acknowledgments: Andrey is especially grateful to Oksana V. Golubova.

Conflicts of Interest: The authors declare no conflicts of interest.

References

1. Rugele, K.; Bumanis, G.; Bajare, D.; Lakevics, V.; Rubulis, J. Alkaline Activated Material for pH Control in Biotechnologies. *Key Eng. Mater.* **2014**, *604*, 223–226. [CrossRef]
2. Gruskevica, K.; Bumanis, G.; Tihomirova, K.; Bajare, D.; Juhna, T. Alkaline Activated Material as the Adsorbent for Uptake of High Concentration of Zinc from Wastewater. *Key Eng. Mater.* **2016**, *721*, 123–127. [CrossRef]
3. Liu, B.; Huang, T.; Zhang, Z.; Wang, Z.; Zhang, Y.; Li, J. The effect of the alkali additive on the highly active Ru/C catalyst for water gas shift reaction. *Catal. Sci. Technol.* **2014**, *4*, 1286. [CrossRef]
4. Novais, R.M.; Buruberri, L.H.; Seabra, M.P.; Bajare, D.; Labrincha, J.A. Novel porous fly ash-containing geopolymers for pH buffering applications. *J. Clean. Prod.* **2016**, *124*, 395–404. [CrossRef]
5. Minkiewicz, J.; Mozgawa, W.; Kr, M. IR spectroscopy studies of zeolites in geopolymeric materials derived from kaolinite. *J. Mol. Struct.* **2016**, *1126*, 200–206.
6. Criado, M.; Fernandez-Jimenez, A.; Torre, G.; Aranda, M.G.; Palomo, A. An XRD study of the effect of the SiO_2/Na_2O ratio on the alkali activation of fly ash. *Cem. Concr. Res.* **2007**, *37*, 671–679. [CrossRef]
7. Duxson, P.; Fernandez-Jimenez, A.; Provis, J.L.; Lukey, G.C.; Palomo, A.; van Deventer, J.S.J. Geopolymer technology: The current state of the art. *J. Mater. Sci.* **2007**, *42*, 2917–2933. [CrossRef]
8. Grutzeck, M.; Kwan, S.; DiCola, M. Zeolite formation in alkali-activated cementitious systems. *Cem. Concr. Res.* **2004**, *34*, 949–955. [CrossRef]
9. Pitcher, S.K.; Slade, R.C.T.; Ward, N.I. Heavy metal removal from motorway stormwater using zeolites. *Sci. Total Environ.* **2004**, *161*, 334–335. [CrossRef]
10. Zamzow, M.J.; Eichbaum, B.R.; Sandgren, K.R.; Shanks, D.E. Removal of Heavy Metals and Other Cations from Wastewater Using Zeolites. *Sep. Sci. Technol.* **1990**, *25*, 1555–1569. [CrossRef]
11. Cooney, E.L.; Booker, N.A. Ammonia Removal from Wastewaters Using Natural Australian Zeolite. II. Pilot-Scale Study Using Continuous Packed Column Process. *Sep. Sci. Technol.* **1999**, *34*, 2741–2760. [CrossRef]
12. Teresa, M.; Deng, S. Ce–Fe-modified zeolite-rich tuff to remove Ba^{2+}-like $^{226}Ra^{2+}$ in presence of As(V) and F^- From aqueous media as pollutants of drinking water. *J. Hazard. Mater.* **2016**, *302*, 341–350.
13. Bumanis, G.; Vitola, L.; Fernandez-Jimenez, A.; Palomo, A.; Bajare, D. The Effect of Heat Treatment on Alkali Activated Materials. *Mater. Sci.* **2017**, *23*, 266. [CrossRef]
14. Kim, J.; Baek, G.; Kim, J.; Lee, C. Energy production from different organic wastes by anaerobic co-digestion: Maximizing methane yield versus maximizing synergistic effect. *Renew. Energy* **2019**, *136*, 683–690. [CrossRef]
15. Rikkonen, P.; Tapio, P.; Rintamäki, H. Visions for small-scale renewable energy production on Finnish farms—A Delphi study on the opportunities for new business. *Energy Policy* **2019**, *129*, 939–948. [CrossRef]

16. Xie, F.; Lin, Z.; Podkaminer, K. Could a bioenergy program stimulate electric vehicle market penetration? Potential impacts of biogas to electricity annual rebate program. *GCB Bioenergy* **2019**, *11*, 623. [CrossRef]
17. Abdul Aziz, N.I.H.; Hanafiah, M.M.; Mohamed Ali, M.Y. Sustainable biogas production from agrowaste and effluents—A promising step for small-scale industry income. *Renew. Energy* **2019**, *132*, 363–369. [CrossRef]
18. Vo, T.T.Q.; Rajendran, K.; Murphy, J.D. Can power to methane systems be sustainable and can they improve the carbon intensity of renewable methane when used to upgrade biogas produced from grass and slurry? *Appl. Energy* **2018**, *228*, 1046–1056. [CrossRef]
19. Rajendran, K.; O'Gallachoir, B.; Murphy, J.D. The combined role of policy and incentives in promoting cost efficient decarbonisation of energy: A case study for biomethane. *J. Clean. Prod.* **2019**, *219*, 278–290. [CrossRef]
20. Lee, W.K.W.; Van Deventer, J.S.J. Use of Infrared Spectroscopy to Study Geopolymerization of Heterogeneous Amorphous Aluminosilicates. *Langmuir* **2003**, *19*, 8726–8734. [CrossRef]
21. Cucchiella, F.; Dadamo, I.; Gastaldi, M. Biomethane: A Renewable Resource as Vehicle Fuel. *Resources* **2017**, *6*, 58. [CrossRef]
22. Zhao, Z.; Cui, X.; Ma, J.; Li, R. Adsorption of carbon dioxide on alkali-modified zeolite 13X adsorbents. *Int. J. Greenh. Gas. Control* **2007**, *1*, 355–359. [CrossRef]
23. Shams, K.; Mirmohammadi, S.J. Preparation of 5A zeolite monolith granular extrudates using kaolin: Investigation of the effect of binder on sieving/adsorption properties using a mixture of linear and branched paraffin hydrocarbons. *Microporous Mesoporous Mater.* **2007**, *106*, 268–277. [CrossRef]
24. Peglow, M.; Antonyuk, S.; Jacob, M.; Palzer, S.; Heinrich, S.; Tsotsas, E. Particle Formulation in Spray Fluidized Beds. In *Modern Drying Technology*; Wiley-VCH Verlag GmbH & Co. KGaA: Weinheim, Germany, 2011; p. 295.
25. Mörl, L.; Heinrich, S.; Peglow, M. Chapter 2 Fluidized bed spray granulation. In *Handbook of Powder Technology*; Elsevier Science: Burlington, MA, USA, 2007; Volume 11, pp. 21–188.
26. Müller, P.; Russell, A.; Tomas, J. Influence of binder and moisture content on the strength of zeolite 4A granules. *Chem. Eng. Sci.* **2015**, *126*, 204–215. [CrossRef]
27. He, Y.; Cui, X.; Liu, X.; Wang, Y.; Zhang, J.; Liu, K. Preparation of self-supporting NaA zeolite membranes using geopolymers. *J. Memb. Sci.* **2013**, *447*, 66–72. [CrossRef]
28. Jin, M.; Liu, L.; Xue-min, C.; Yan, H.; Chen, J.; Liu, X. The hydrothermal transformation of solid geopolymers into zeolites. *Microporous Mesoporous Mater.* **2012**, *161*, 187–192.
29. Lee, N.K.; Choudhry, I.; Lee, H.K.; Wang, Z.; Khalid, H.R. Evolution of zeolite crystals in geopolymer-supported zeolites: Effects of composition of starting materials. *Mater. Lett.* **2018**, *239*, 33–36.
30. Provis, J.L.; Van Deventer, J.S.J. *Alkali Activated Materials: State-of-the-Art Report, RILEM TC 224-AAM*; Springer: Dordrecht, The Netherlands, 2014; Volume 13, p. 388.
31. Wang, J.; Ge, Y.; He, Y.; Xu, M.; Cui, X. A porous gradient geopolymer-based tube membrane with high PM removal rate for air pollution. *J. Clean. Prod.* **2019**, *217*, 335–343. [CrossRef]
32. Xu, M.; He, Y.; Liu, Z.; Tong, Z.; Cui, X. Preparation of geopolymer inorganic membrane and purification of pulp-papermaking green liquor. *Appl. Clay Sci.* **2019**, *168*, 269–275. [CrossRef]
33. Innocentini, M.D.M.; Botti, R.F.; Bassi, P.M.; Paschoalato, C.F.P.R.; Flumignan, D.L.; Franchin, G.; Colombo, P. Lattice-shaped geopolymer catalyst for biodiesel synthesis fabricated by additive manufacturing. *Ceram. Int.* **2019**, *45*, 1443–1446. [CrossRef]
34. Zheng, Z.; Ma, X.; Zhang, Z.; Li, Y. In-situ transition of amorphous gels to Na-P1 zeolite in geopolymer: Mechanical and adsorption properties. *Constr. Build. Mater.* **2019**, *202*, 851–860. [CrossRef]
35. Khalid, H.R.; Lee, N.K.; Park, S.M.; Abbas, N.; Lee, H.K. Synthesis of geopolymer-supported zeolites via robust one-step method and their adsorption potential. *J. Hazard. Mater.* **2018**, *353*, 522–533. [CrossRef] [PubMed]
36. Minelli, M.; Medri, V.; Papa, E.; Miccio, F.; Landi, E.; Doghieri, F. Geopolymers as solid adsorbent for CO_2 capture. *Chem. Eng. Sci.* **2016**, *148*, 267–274. [CrossRef]
37. Papa, E.; Medri, V.; Amari, S.; Manaud, J.; Benito, P.; Vaccari, A.; Landi, E. Zeolite-geopolymer composite materials: Production and characterization. *J. Clean. Prod.* **2018**, *171*, 76–84. [CrossRef]
38. Minelli, M.; Papa, E.; Medri, V.; Miccio, F.; Benito, P.; Doghieri, F.; Landi, E. Characterization of novel geopolymer—Zeolite composites as solid adsorbents for CO_2 capture. *Chem. Eng. J.* **2018**, *341*, 505–515. [CrossRef]

39. Papa, E.; Medri, V.; Paillard, C.; Contri, B.; Natali Murri, A.; Vaccari, A.; Landi, E. Geopolymer-hydrotalcite composites for CO_2 capture. *J. Clean. Prod.* **2019**, *237*, 117738. [CrossRef]
40. Medri, V.; Papa, E.; Lizion, J.; Landi, E. Metakaolin-based geopolymer beads: Production methods and characterization. *J. Clean. Prod.* **2019**. [CrossRef]
41. Özen, S.; Alam, B. Compressive Strength and Microstructural Characteristics of Natural Zeolite-based Geopolymer. *Period. Polytech. Civ. Eng.* **2017**, *62*, 64–71. [CrossRef]
42. Zhang, Z.; Wang, H.; Provis, J.L.; Bullen, F.; Reid, A.; Zhu, Y. Quantitative kinetic and structural analysis of geopolymers. Part 1. The activation of metakaolin with sodium hydroxide. *Thermochim. Acta* **2012**, *539*, 23–33. [CrossRef]
43. Garcia-Lodeiro, I.; Fernandez-Jimenez, A.; Blanco, M.T.; Palomo, A. FTIR study of the sol-gel synthesis of cementitious gels: C–S–H and N–A–S–H. *J. Sol.-Gel Sci. Technol.* **2008**, *45*, 63–72. [CrossRef]
44. Criado, M.; Palomo, A. Fernandez-Jimenez, A. Alkali activation of fly ashes. Part 1: Effect of curing conditions on the carbonation of the reaction products. *Fuel* **2005**, *84*, 2048–2054. [CrossRef]
45. Palomo, A.; Blanco-varela, M.T.; Granizo, M.L.; Puertas, F.; Vazquez, T.; Grutzeck, M.W. Chemical stability of cementitious materials based on metakaolin. *Cem. Concr. Res.* **1999**, *29*, 997–1004. [CrossRef]
46. Ugal, J.R.; Mustafa, M.; Abdulhadi, A.A. Preparation of Zeolite Type 13X from Locally Available Raw Materials. *51 Iraqi J. Chem. Pet. Eng.* **2008**, *9*, 51–56.
47. Brunauer, S.; Emmett, P.H.; Teller, E. Adsorption of Gases in Multimolecular Layers. *J. Am. Chem. Soc.* **1938**, *60*, 309–319. [CrossRef]